A simulation study on the effect of sodium on grain boundary passivation in CIGS thin-film solar cells

A simulation study on the effect of sodium on grain boundary passivation in CIGS thin-film solar cells

Giovanna Sozzi[1], Oana Cojocaru-Mirédin[2] and Roland Wuerz[3]

[1]Department of Engineering and Architecture, University of Parma, Parco Area delle Scienze 181A, 43124 Parma, Italy

[2]RWTH Aachen, Physikalisches Institut IA, Sommerfeldstr. 14, 52074 Aachen, Germany

[3]Zentrum für Sonnenenergie- und Wasserstoff-Forschung Baden-Württemberg (ZSW), Meitnerstraße 1, 70563 Stuttgart, Germany

***Abstract*—3D numerical simulations of CIGS thin-film solar cells with different grain-boundary (GB) characteristics have been carried out in order to investigate the effect of defect properties and band edge shifts at GBs on the cell performance. Simulation results are compared with experimental data taken on cells with and without NaF post deposition treatment. GBs with different energy gaps and defect properties have been analyzed. Simulations support the idea that the detrimental effect of defective GBs on the cell performance might be reduced by a treatment with Na. The results of this study can help with the interpretation of experimental findings.**

Keywords—CIGS, Cu-depletion, defect passivation, grain boundary, Na treatment.

I. Introduction

Polycrystalline CIGS solar cells have achieved power efficiency conversion above 23% [1], despite the presence of numerous grain-boundaries (GBs). The role and physics of GBs has thus received considerable attention, but how exactly the GBs affect the efficiency of the cells is still under debate.

In order to obtain such high performance, the CIGS has to be doped with alkali metals: in particular, the effect of Na in CIGS solar cells has been widely discussed in the literature [2], but although Na has been directly observed at GBs [3], the underlying reasons for the improvement of cell efficiency have not yet been fully understood.

Investigations by atom probe tomography (APT) have recently shown that Na segregation, Cu depletion and In accumulation at GB are common traits of beneficial GBs that can promote the carrier collection and separation [3], similarly to the GB characteristics observed in high efficiency cells [4].

To gain further insight into the role of GBs on the cell performance, the present study focuses in particular on the effect of defects and band edge shifts at GBs on the cell performance. Results provided by modelling can help to comprehend the role of GBs in solar cells treated with Na, and lead to better interpretation of experimental data.

II. Experiments And Methods

Experimental data are taken on Na-containing and Na-free CIGS cells manufactured by ZSW on ZrO_2 substrates [5]. The solar cells feature a p-type CIGS absorber of about 2 µm without Ga grading, an n-type CdS buffer of 60 nm, 80 nm of intrinsic ZnO and about 400 nm of Al-doped ZnO as transparent conductive oxide layer with molybdenum as rear contact and nickel/aluminum/nickel electrodes as front contact. No anti-reflecting coating has been used. The bandgap as derived from quantum efficiency measurements was 1.19 eV for both, the Na-free and Na-doped sample.

The 3D model of the cell sketched in Fig.1 considers a cylindrical CIGS grain with 200 nm radius surrounded by the grain boundary. The GB is modeled as a thin region, 2 nm wide, decorated by donor defects. Since different defect activation energies, E_A, have been measured in the cells with and without Na post-deposition treatment (PDT) [5], the effect on the cell performance of defects with E_A=160, 300 and 350 meV is investigated. Recombination via defects follows the SRH model as detailed in [6].

Besides the different defect population, the GB may differ from the grain interior (GI) by a larger bandgap due to Cu depletion [7]; cells with E_{g_GB} = 1.23, 1.29 and 1.34 eV at the GB are simulated [8].

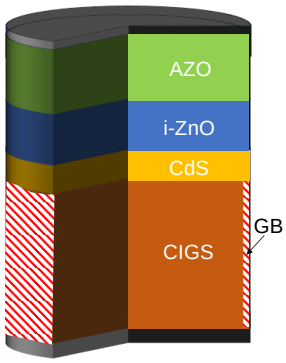

Fig. 1. Simulated cells structure. Red-hatched region indicates the GB.

All simulations are performed with the Synopsys Sentaurus-Tcad suite, at room temperature, both in dark and under AM1.5G illumination. The light propagation through the layered media is calculated by the transfer matrix method (TMM); the optical generation in the CIGS is calculated on the basis of complex refractive indexes depending on both the [Ga]/([Ga]+[In]) and [Cu]/([Ga]+[In]) ratios [9,10].

The conduction-band offsets at ZnO/CdS and CdS/CIGS that can affect the current behavior, as explained in [11], have been set at -0.2 eV and 0.1 eV respectively, while the other main cell parameter values can be found in [12].

III. Results And Discussion

A. *Modelling of Na-doped Cell*

At first, a cell with an energy gap $E_{g\text{-}GB}$ of 1.19 eV in the GI and GB has been simulated. In this case, the GB only differs from the GI by the presence of donor traps with an activation energy of 160 meV, as measured for Na-doped samples [5].

A Gaussian energy distribution is required for good fitting of simulated current-voltage (IV) curves and experimental data both in dark and under illumination. The simulated IV curve (black dashed line) for a donor defect peak value of $7\cdot10^{18}$ $eV^{-1}cm^{-3}$, a hole capture cross section at GB of $4\cdot10^{-17}cm^2$, is shown in Fig. 2, together with measured ones (green solid lines, measured on 5 different cells of Na-doped sample).

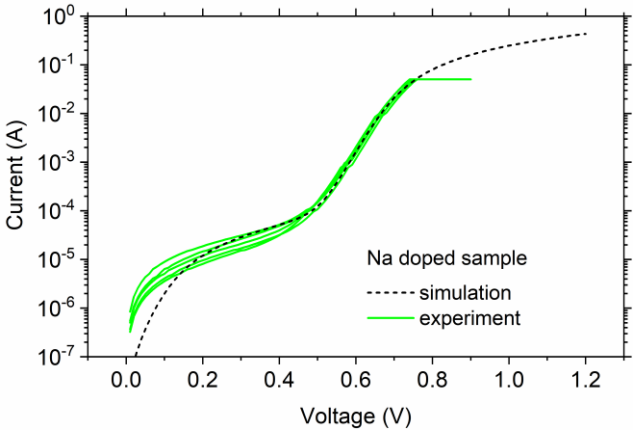

Fig. 2. Measured and simulated dark current-voltage curve for Na-doped cell (as described in the text).

The corresponding simulated cell parameters show an excellent agreement with the mean values of the measured figures of merits (see Table I).

Using this model as the reference cell, the effect of different measured trap activation energies and energy gaps in the GB on the cell performance have been evaluated.

TABLE I. Measured And Simulated Cell Parameters (Na-Doped Cell).

	Voc (mV)	Jsc (mA/cm²)	FF(%)	η (%)
IV Measurement	668	29.67	78.30	15.53
Simulation	669	29.69	78.30	15.55

B. *Effect of Cu depletion at GBs*

In order to evaluate the potential impact of Cu depletion on the cell efficiency, the following points have been considered:

(i) it is known from APT measurements that the GB is Cu depleted, but the value of E_g at the GB depends on the degree of Cu depletion and GB composition [8];

(ii) it is also known that the enlargement of E_g in Cu depleted GBs is primarily determined by a downshift of the valence band [7], that causes a valence band offset, ΔE_v, at the GI/GB;

iii) simulation studies [13] have shown that a valence band offset, ΔE_v, between the GI and the GB is equivalent to have an hole effective capture cross-section, $\sigma_{h\text{-}eff}$, of the trap in the GB given by:

$$\sigma_{h\text{-}eff}=\sigma_h \exp(-\Delta E_v/kT) \quad (1)$$

where σ_h is the trap hole capture cross section, k the Boltzmann constant and T the temperature. In this respect, the capture cross section used in the reference cell model can be considered as $\sigma_{h\text{-}eff}$, since no E_g enlargement has been initially modeled at GBs.

The *real* hole capture cross section of the trap in the GB, σ_h, can thus be calculated with (1) from the value $\sigma_{h\text{-}eff}=4\cdot10^{-17}$ cm^2 used in the reference cell to fit the experimental data, and depends on the value of E_g at the GB, that is to say the degree of Cu depletion.

Cells with E_g = 1.19, 1.23, 1.29 and 1.34 eV at the GB corresponding to ΔE_v =0, 40, 100 and 150 meV, respectively, have been simulated; for each value of E_g, the hole capture cross section of defect in the GB has been calculated accordingly to (1), with $\sigma_{h\text{-}eff}=4\cdot10^{-17}$ cm^2. The simulated data reported in Table II, demonstrate that the same cell photovoltaic (PV) parameters of the reference cell can also be obtained with traps of larger cross section in combination with larger ΔE_v at the GI/GB interface, that is to say Cu-depletion at GBs can improve the performance of cells.

TABLE II. Simulated Cell Parameters For Different Eg and ΔE_V At GB. σ_H Is Calculated From $\sigma_{H\text{-}EFF}$ With (1). E_G = 1.19, 1.23, 1.29 and 1.34 eV At The GB Correspond To ΔE_v =0, 40, 100 And 150 meV. Defect Activation Energy E_A = 160 meV (See Text For Details).

σ_h (cm^2)	$\sigma_{h\text{-}eff}$ (cm^2)	ΔE_V (meV)	Voc (mV)	Jsc (mA/cm²)	FF (%)	η (%)
$4\cdot10^{-17}$	$4\cdot10^{-17}$	0	669	29.69	78.30	15.55
$1.9\cdot10^{-16}$	$1.9\cdot10^{-16}$	0	663	29.01	77.85	14.97
	$4\cdot10^{-17}$	40	669	29.66	78.28	15.54
$1.9\cdot10^{-15}$	$1.9\cdot10^{-15}$	0	628	22.88	73.74	10.60
	$4\cdot10^{-17}$	100	669	29.63	78.28	15.52
$1.3\cdot10^{-14}$	$1.3\cdot10^{-14}$	0	571	9.28	64.83	3.44
	$4\cdot10^{-17}$	150	669	29.6	78.28	15.50

In particular, recombination at GBs is largely suppressed by the valence band offset that impedes holes to reach the defective GB region and recombine there, as shown in Fig. 3 by the valence

bands and SRH recombination profiles at short circuit condition for σ_h=1.3·10^{-14} cm^2 and ΔE_V = 0, 150 meV (see Table II).

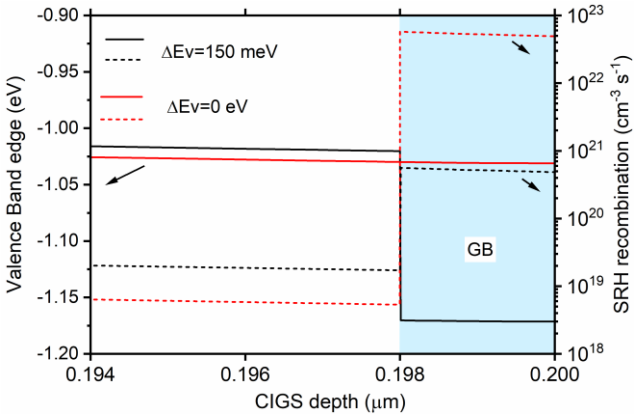

Fig. 3. Valence Band (solid line) and SRH recombination profiles (dashed lines) along a horizontal line in the middle of CIGS at short circuit condition, for a defect at GB with E_A = 160 meV.

C. *Effect of defect activation energy at GBs*

In the sample without NaF post-deposition treatment, an additional defect with an activation energy of 300-350 meV has been detected [5].

In order to evaluate the effect of a trap with different activation energy on the cell performance, the cell figures of merit have been simulated for a defect located at 300 and 350 meV below the conduction band edge, for each values of σ_h calculated in section B. Data are reported in Table III for the case of no E_g enlargement at the GB (i.e., E_{g_GB} = 1.19 eV, ΔE_v=0 eV, the worst case for the cell performance).

TABLE III. SIMULATED CELL PARAMETERS FOR DIFFERENT ACTIVATION ENERGY, E_A= E_C-E_T, OF DEFECT AT GB. E_G=1.19 EV @ GB (I.E., ΔE_V=0 EV).

σ_h (cm^2)	E_C-E_T (meV)	Voc (mV)	Jsc (mA/cm^2)	FF (%)	η (%)
4·10^{-17} (reference cell)	**160**	**669**	**29.69**	**78.30**	**15.55**
1.9·10^{-16}	160	663	29.01	77.85	14.97
	300	588	30.85	74.58	13.53
	350	568	31.36	67.82	12.08
1.9·10^{-15}	160	628	22.88	73.74	10.60
	300	522	22.47	67.12	7.88
	350	504	22.86	59.3	6.83
1.3·10^{-14}	160	571	9.28	64.83	3.44
	300	451	7.26	58.72	1.92
	350	431	6.43	53.65	1.49

It is apparent from simulation results in Table III, that the increased recombination at GBs in the case of deep trap and large capture cross section is consistent both with the reduction of V_{oc} and FF experimentally observed in the Na-free cells [5].

However, differently from simulation results, no reduction of J_{sc} is measured in the cell without NaF PDT, despite the presence of a deep defect with activation energy of 300-350 meV.

However, if the energy gap enlargement at the GB due to Cu depletion is accounted for in the model, the effects of the defect at the GB on the cell's parameters change (see Table IV).

In particular, simulations demonstrate that even in the presence of large concentration of deep defects, the J_{sc} does not reduce if the GB has a sufficient large energy gap compared to the GI. This behavior can be related to variations in the SRH recombination, as shown in Fig. 4 for σ_h=1.3·10^{-14} cm^2.

TABLE IV. SIMULATED CELL PV PARAMETERS FOR ACTIVATION ENERGY E_C- E_T=350 MEV OF DEFECT AT GB. ΔE_V@GB AND σ_H WERE VARIED.

σ_h (cm^2)	ΔE_V@GB (meV)	Voc (mV)	Jsc (mA/cm^2)	FF (%)	η (%)
1.9·10^{-16}	0	568	31.36	67.82	12.08
	40	607	32.08	70.3	13.69
1.9·10^{-15}	0	504	22.86	59.3	6.83
	100	607	32.04	70.3	13.68
1.3·10^{-14}	0	431	6.43	53.65	1.49
	150	608	32.0	70.31	13.67

In fact, in the case of ΔE_V = 0 eV (black squares), the recombination at the GB is very large and J_{sc} is drastically reduced; for ΔE_V = 150 meV (red circles) instead, the large valence band offset, ΔE_v, arising at the GI/GB interface acts as a hole barrier, and J_{sc} recovers, as explained in sec. II B: as an example, in the case of defect with E_A = 350 meV, the mean SRH recombination rate in the GB drops from 4.29·10^{22} to 3.34·10^{20} cm^{-3}s^{-1} and the current raises from 6.43 to 32 mA/cm^2.

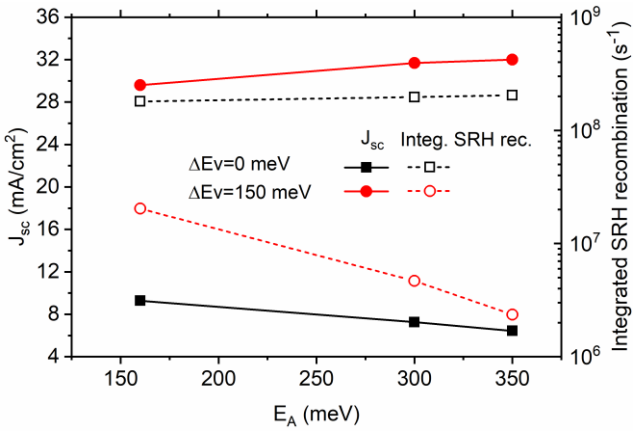

Fig. 4 Short circuit current density (full symbols) and SRH recombination (open symbols) in the CIGS layer for ΔE_V = 0 (black symbols) and 150 meV (red symbols), variable trap activation energies, E_A = 160, 300, 350 meV and hole capture cross section σ_h=1.3·10^{-14} cm^2.

Fig.4 also shows a different dependence of J_{sc} on E_A depending on the value of ΔE_V. This behavior can be explained as follows.

Due to the very large SRH recombination rate at the GB for $\Delta E_V = 0$ eV, the integrated recombination in the grain-boundary exceeds that in the grain interior despite the small GB volume: J_{sc} thus reduces with E_A, since the deeper the defect in the energy gap the larger the recombination (lines with squares in Fig. 4). In the case of large ΔE_V (lines with circles in Fig. 4), recombination at GB drops due to the ΔE_V arising at GI/GB interface, and can become comparable with that in the GI that has a lower recombination rate but a larger volume than the GB.

On the other hand, the ionized donor concentration in the GB diminishes with E_A too and affects the carrier concentration in the GI region next to GB (Fig.5a), where the carrier recombination velocity reduces (Fig. 5b).

While the recombination at the GB tends to increase with E_A, the one in the GI behaves in the opposite way, therefore the final trend of recombination as a function of E_A will depend on which of them dominates.

In the case of $\Delta E_V = 150$ meV the recombination in the GB does not vary much with the trap activation energy (see Fig.5b), so that the overall recombination in the CIGS reduces with E_A and the J_{sc} increases (full circles in Fig. 4).

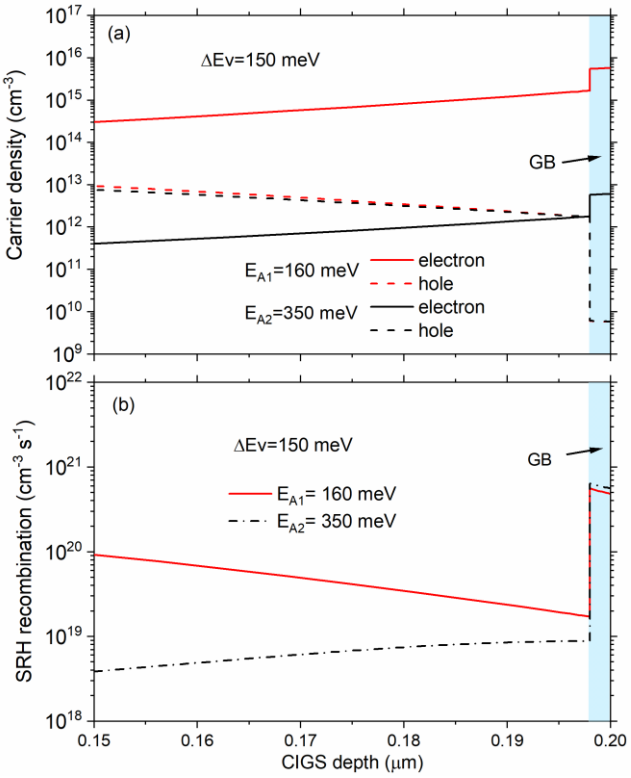

Fig. 5. a) Carrier density and b) SRH recombination rate along a horizontal line in the middle of CIGS at short circuit condition for a defect at the GB with activation energy $E_{A1} = 160$ meV and $E_{A2} = 350$ meV.

D. Effect of two defects at the GB with $E_{A1} = 160$ meV and $E_{A2} = 350$ meV

DLTS and TAS analysis of Na-free cells [5], have detected the simultaneous presence of two defects. One with an activation energy of $E_c - E_{T1} = E_{A1} = 160$ meV, as in the Na containing sample, and one with $E_c - E_{T2} = E_{A2} = 300$-$350$ meV.

The simulation results for the scenario of two defects at GB with activation energies 160 meV and 350 meV and the same gaussian distribution in energy used in the Na-doped cell, are shown in Fig. 6 for different values of the hole capture cross section, σ_{h_deep}, of the defect with $E_A = 350$ meV; $E_{g\_GB} = 1.34$ eV, i.e. $\Delta E_V = 150$ meV.

Simulations show that a $\sigma_{h\_deep} \geq 10^{-12}$ cm^2 is required to reach an efficiency as low as the one measured in the Na-free cell, i.e., $\eta = 8.84$ %. On the other hand, the J_{sc} corresponding to such $\sigma_{h\text{-}deep}$ is lower and the V_{oc} and FF are larger than the cell parameters measured in the Na-free cell that are summarized in Table V.

A possible reason for this discrepancy might be that, except for the different activation energies, both traps at the GB have been simulated with the same Gaussian distribution in energy as in the case of the Na-doped cell, i.e, peak concentration of $7 \cdot 10^{18}$ eV^{-1}cm^{-3} and standard deviation of 0.05 eV.

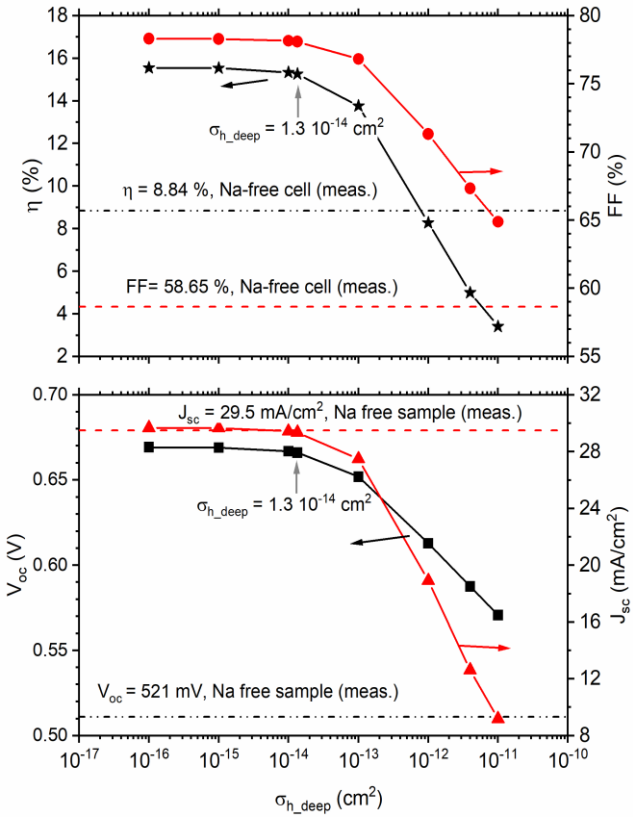

Fig. 6. Cell's parameters, in the case of two defects in the GB, versus the hole capture cross section, σ_{h_deep}, of defect with $E_{A2} = 350$ meV, and $N_{T2} = 7 \cdot 10^{18}$ eV^{-1}cm^{-3}. The shallow defect has an $E_{A1} = 160$ meV and $N_{T1} = 7 \cdot 10^{18}$ eV^{-1}cm^{-3} (more details on defects' properties in the text). $\Delta E_V = 150$ meV.

Instead, a good agreement has been obtained between simulated and measured PV parameters in the case of Na-free cells by decorating the GB with the two defects (i.e., with E_A = 160 meV and E_{A2} = 350 meV), but with different characteristics.

In particular, a peak trap concentration of $1.85 \cdot 10^{18}$ $eV^{-1}cm^{-3}$ for the shallower defect, and $9 \cdot 10^{17}$ $eV^{-1}cm^{-3}$ for the deeper one, and a $\sigma_{h\_deep} = 1.4\ 10^{-11}$ cm^2 allows to obtain a reduction of the V_{oc}, FF and η with almost no degradation of the J_{sc}, compared to the Na-doped cell, as in measurements (see Table V).

The way the two defects affect the cell performance is worth further investigation, however, this example would seem to suggest a possible effect of the Na treatment on the electronic properties of GBs.

TABLE V. MEASURED AND SIMULATED CELL PV PARAMETERS FOR ΔE_V =150 MEV.

	E_A (meV)	N_T (eV^{-1} cm^{-3})	σ_h (cm^2)	V_{oc} (mV)	J_{sc} (mA/cm^2)	FF (%)	η (%)
Na-free							
IV Meas.	-			511	29.50	58.65	8.84
Sim.	160	$1.85 \cdot 10^{18}$	$1.3 \cdot 10^{-14}$	515	29.66	57.48	8.78
	350	$0.9 \cdot 10^{18}$	$1.4 \cdot 10^{-11}$				
Na-doped							
IV Meas.	-			668	29.67	78.30	15.53
Sim.	160	$7 \cdot 10^{18}$	$1.3 \cdot 10^{-14}$	669	29.6	78.28	15.50
	350	0	-				

IV. CONCLUSIONS

3D numerical simulations of solar cells with different GB characteristics have been carried out in order to investigate the effect of defect properties and band edge shifts at GBs on the cell performance.

Starting from the experimental evidence of Cu-depletion and Na segregation at grain boundaries, GBs with different energy gaps and defect properties have been studied. Simulations prove that the band gap widening due to Cu depletion at GBs can help salvaging the performance of cells otherwise limited by non-radiative recombination at GBs.

GBs with defect activation energies measured in Na-free and Na-doped cells have been also simulated. Introduction of a deep level in the GB can explain the reduction of V_{oc} and FF of Na-free cells, but the simulated J_{sc} suppression is not consistent with the experimental data. By the introduction of a valence band offset at the GB, J_{sc} remains unaffected by the deep level as observed experimentally.

In Na-free cells, measurements have detected the simultaneous presence of two defects, one with activation energy of $E_{A1} = E_c - E_{T1}$ = 160 meV, as observed in the Na containing samples, and one with $E_{A2} = E_c - E_{T2}$ = 300-350 meV, only detected in the Na-free sample.

A reduction of the V_{oc}, FF and η with almost no degradation of the J_{sc} as the ones measured in Na-free solar cells can be simulated by considering both shallow and deep defects at the GB, but with different concentration compared to the case of Na-doped cell. This might suggest the positive effect of the Na treatment on the electronic properties of GBs.

ACKNOWLEDGEMENT

We gratefully acknowledge support by the Deutsche Forschungs-Gemeinschaft (Contract No. WU 693/2-1).

REFERENCES

[1] "Solar Frontier hits new CIS cell efficiency record – pv magazine International." [Online]. Available: https://www.pv-magazine.com/2019/01/21/solar-frontier-hits-new-cis-cell-efficiency-record/. [Accessed: 23-Jan-2021].

[2] Y. Sun et al., "Review on Alkali Element Doping in Cu(In,Ga)Se2 Thin Films and Solar Cells," Engineering, vol. 3, no. 4, pp. 452–459, 2017.

[3] M. Raghuwanshi, R. Wuerz, and O. Cojocaru-Mirédin, "Interconnection between Trait, Structure, and Composition of Grain Boundaries in Cu(In,Ga)Se2 Thin-Film Solar Cells," Adv. Funct. Mater., vol. 30, no. 31, pp. 1–9, 2020.

[4] M. Raghuwanshi et al., "Influence of RbF post deposition treatment on heterojunction and grain boundaries in high efficient (21.1%) Cu(In,Ga)Se2 solar cells," Nano Energy, vol. 60, no. March, pp. 103–110, 2019.

[5] A. Czudek, A. Eslam, A. Urbaniak, P. Zabierowski, R. Wuerz, and M. Igalson, "Evolution of the electrical characteristics of Cu(In,Ga)Se2devices with sodium content," J. Appl. Phys., vol. 128, no. 17, 2020.

[6] G. Sozzi, R. Mosca, M. Calicchio, and R. Menozzi, "Anomalous dark current ideality factor (n > 2) in thin-film solar cells: The role of grain-boundary defects," in 2014 IEEE 40th Photovoltaic Specialists Conference, PVSC 2014, pp.1718-1721, 2014.

[7] C. Persson and A. Zunger, "Compositionally induced valence-band offset at the grain boundary of polycrystalline chalcopyrites creates a hole barrier," Appl. Phys. Lett., vol. 87, no. 21, pp. 1–3, 2005.

[8] M. Tsuyoshi, G. Weiyan, and W. Takahiro, "Crystallographic and optical properties and band structures of CuInSe 2 , CuIn3Se5 , and CuIn5Se8 phases in Cu-poor Cu2Se–In2Se3 pseudo-binary system" Jpn. J. Appl. Phys., vol. 55, no. 4S, p. 04ES15, 2016.

[9] G. Sozzi et al., "Analysis of Ga grading in CIGS absorbers with different Cu content," in 43rd IEEE Photovoltaic Specialists Conference, PVSC 2016, pp. 2279-2282, 2016.

[10] R. Carron et al., "Refractive indices of layers and optical simulations of Cu (In , Ga) Se 2 solar cells," Sci. Technol. Adv. Mater., vol. 6996, pp. 1–15, 2018.

[11] G. Sozzi et al., "Influence of Conduction Band Offsets at Window/Buffer and Buffer/Absorber Interfaces on the Roll-Over of J-V Curves of CIGS Solar Cells," in 2017 IEEE 44th Photovoltaic Specialists Conference, PVSC 2017, pp. 2205–2208, 2017.

[12] G. Sozzi et al., "Designing CIGS solar cells with front-side point contacts," in 2015 IEEE 42nd Photovoltaic Specialists Conference, PVSC 2015, Art. no. 7355691, pp. 1–5, 2015.

[13] K. Taretto, U. Rau, K. Taretto, and U. Rau, "Numerical simulation of carrier collection and recombination at grain boundaries in Cu(In , Ga) Se2 solar cells," J. Appl. Phys., vol. 094523, no. May 2013, 2008.